Arabian Journal for Science and Engineering (2025) 50:4197–4207
https://doi.org/10.1007/s13369-024-09586-2

RESEARCH ARTICLE-CHEMICAL ENGINEERING

Hybrid Nanoparticle-Enhanced Fluid Flow and Heat Transfer Behaviors in a Parabolic Cavity with a Heat Source

Rasul Mohebbi[1] · **Yuan Ma**[2]

Received: 19 March 2024 / Accepted: 9 September 2024 / Published online: 23 September 2024

Abstract
Natural convection of nanofluids holds considerable importance in both scientific research and engineering applications due to their exceptional heat transfer capabilities, which occur spontaneously without the need for additional energy input. In this paper, the natural convection of nanofluid inside a parabolic cavity containing a hot obstacle is studied numerically. The shape of the hot obstacle is selected as either circular or elliptical. Additionally, the effects of the Rayleigh number, nanoparticle volume fraction, and the position of the heat source are investigated. The computational fluid dynamics model was computed using COMSOL Multiphysics. It is observed that the average Nusselt number tends to increase with both the Rayleigh number and the volume fraction of nanoparticles in the fluid. When the heat source moves from the bottom region to the top area, the heat transfer performance of the heat source increases. When $Ra \leq 10^5$, the cases with circular heat sources exhibit better heat transfer performance than those with elliptical heat sources. However, at $Ra = 10^6$, the average Nusselt number of the elliptical heat source is higher than that of the circular one.

Keywords Nanofluid · Parabolical cavity · Heat source · Elliptic

1 Introduction

Improving heat transfer efficiency is crucial not only for increasing energy utilization but also for reducing environmental pollution [1, 2]. The improvement in heat transfer efficiency of a system is limited by the thermal properties of the heat transfer fluid. Therefore, it is essential to explore heat transfer fluids with excellent thermal properties to enhance heat transfer efficiency. Nanofluid is a composite material formed by suspending nanoparticles in a base fluid. These nanoparticles can be made of various nanomaterials, such as metals, oxides, or carbon nanotubes. Nanofluid possesses many unique properties, such as enhanced thermal conductivity, improved rheological properties, and higher surface activity.

✉ Yuan Ma
yuan1ma@polyu.edu.hk

[1] School of Engineering, Damghan University, P.O. Box: 3671641167, Damghan, Iran

[2] Department of Civil and Environmental Engineering, The Hong Kong Polytechnic University, Hong Kong SAR, People's Republic of China

Due to their excellent thermal properties, nanofluids are widely utilized in the field of heat transfer. Yadav et al. [3] performed experiments and numerical simulations to study the Fe_3O_4/water nanofluid heat transfer in a tube. Ma et al. [4] compared the heat transfer performances of Al_2O_3/water and TiO_2/water nanofluids natural convection inside a U-shaped enclosure. The results indicate that for nanoparticles with identical diameters, Al_2O_3 exhibits greater effectiveness than TiO_2 in enhancing heat transfer. Furthermore, additional types of nanoparticles, such as CuO[5], Cu[6], clove-treated graphene nanoplatelet [7], and ZnO [8], have also been investigated in this study.

Besides nanofluids composed of a single type of nanoparticle, those consisting of two or more types are referred to as hybrid nanofluids. Al_2O_3-MWCNT/water hybrid nanofluid has been used by Giwa et al. [9] to enhance the heat transfer performance in a differentially heated square enclosure. The integration of hybrid nanofluids has been noted to improve both the thermal and flow characteristics of the base fluid. As a result, the natural convection behavior of this novel category of nanofluids is improved. Goudarzi et al. [10] analyzed the effect of nanoparticle migration on the natural convection behavior of Ag-MgO/Water hybrid nanofluid. The findings

of the study demonstrate that an increase in thermophoresis diffusion for both types of nanoparticles leads to an 11% increase in the Nusselt number. Reddy et al. [11] numerically studied the Ag-TiO_2/water hybrid nanofluid natural convection in an inclined cavity. The Zn-TiO2/water hybrid nanofluid is used by Yasir et al. [12] to enhance the mixed convective flow. The results from their investigation suggest that the mixed convection parameter exerts a positive influence on rate of heat transport for the upper branch while exerting a negative influence on these factors for the lower branch.

In recent years, there has been increasing attention on natural convection inside wavy enclosures, attributed to the complexity and variability of the boundary. Chuhan et al. [13] investigated the influence of an inclined magnetic field on entropy generation within natural convective flow in a wavy enclosure filled with a non-Newtonian Casson fluid. They discovered that there is an inverse correlation between the Nusselt number and Lewis number, while the Sherwood number demonstrates a positive correlation with the Lewis number. Rashid et al.[14] conducted a numerical investigation on the mass and heat transfer characteristics of magnetohydrodynamic (MHD) Casson fluid flow within a wavy cavity containing a circular heat source. They observed that the heat and mass transfer rates decreased as the Hartmann number increased. Roy and Monira [15] conducted a study on the natural convection behavior of a reacting hybrid nanofluid within an open porous cavity featuring vertical wavy walls while considering the effects of an inclined magnetic field. They observed that regardless of the parameter values, the streamlines within the cavity formed two counter-rotating cells, with the highest intensities occurring near the open end. Geridonmez and Atilgan [16] utilized machine learning modeling to obtain the average Nusselt number, which resulted from numerical simulations of the natural convection of nanofluid in a wavy cavity. Their findings reveal that trilayer neural network modeling is a feasible alternative for obtaining immediate and expected outcomes, as opposed to repeatedly performing numerical simulations for the average Nusselt number at specific parameter settings. Alazzam et al. [17] performed a numerical investigation on the natural convection of NePCM confined within a wavy enclosure. Saha et al. [18] nanofluid natural convection inside a cavity with a top wavy wall and a heated single fin.

Conversely, natural convection within cavities containing internal heat sources has found widespread applications and is gaining increasing attention. Nabwey et al. [19] conducted a numerical investigation of natural convective flow in an inclined wavy porous cavity filled with a square obstacle. Kumar and Mahapatra [20] conducted an experimental and numerical analysis focusing on natural convection within a partially open enclosure containing a cylindrical obstacle. Franco et al. [21] explored the impacts of discrete conductive blocks on natural convection within an open cavity. Their findings revealed that as the solid is progressively diminished in size and augmented in quantity, it hampers the growth of the boundary layer along the hot wall, thereby causing a decrease in the heat transfer process.

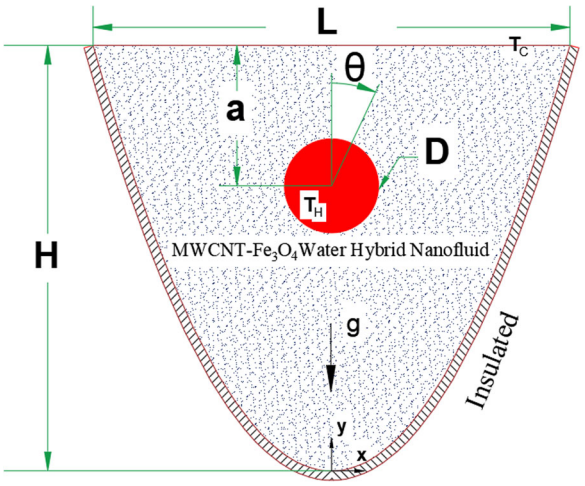

Fig. 1 Schematic diagram of nanofluid natural convection inside a parabolic-shaped enclosure with an obstacle

To the author's knowledge, no prior research exists on the natural convection of nanofluids within a parabolic-shaped cavity containing a circular heat source. Nonetheless, exploring this phenomenon holds considerable significance owing to the distinctive surface boundary of the parabolic cavity [22, 23]. Moreover, the coupling effect between internal heat sources and nanofluids is expected to significantly influence both flow patterns and heat transfer processes. This study investigates the natural convection of nanofluids within a parabolic-shaped cavity featuring a circular heat source. We examine the impacts of Rayleigh number (Ra), volume fraction of nanoparticles, positions, and shapes of obstacles on flow characteristics and heat transfer rates.

2 Physical and Mathematical Depiction

Figure 1 shows the schematic diagram of the present work. As seen in this figure, a heat source is placed inside a parabolic-shaped enclosure. It is worth noting that, in the current study, the heat source has two shapes: circular and elliptical.

The MWCNT-Fe_3O_4/water hybrid nanofluid is used in the present work to enhance the heat transfer performance. The parabolic shape of the cavity is determined by the following equation:

$$Y = \left(\frac{2H}{L}\right)^2 \frac{X^2}{H} \tag{1}$$

where H represents the height of the cavity, and L represents the width of the cavity.

As illustrated in the figure, the heat source is located at the position along the central axis of the cavity, at a distance (a) from the upper wall. The top wall surface of the cavity serves as the cold wall, with a fixed temperature of T_c. The heat source surface is also set at a fixed temperature, T_h. The remaining walls, which are the curved surfaces of the cavity, serve as adiabatic walls.

3 Numerical Method and Strategy

When the fluid is subjected to non-uniform temperature and gravity fields, it often exhibits natural convective transport phenomena observed in various real-world scenarios. This natural phenomenon drives the circulation of fluids and the transfer of energy within a system. Specifically, the Boussinesq approximation can govern fluid and heat transport in the system by utilizing continuity, momentum, and energy equations. These equations describe the relationships between various parameters such as the velocity vector (**u**), density of the nanofluid (ρ_{nf}), time (t), pressure (p), dynamic viscosity of nanofluid (μ_{nf}), thermal conductivity of nanofluid (k_{nf}), specific heat capacity at constant pressure (C_p), and the local (T) and reference temperatures (T_r). By analyzing and understanding these equations, we can gain valuable insights into the dynamics of the natural convective transport phenomenon and how it affects fluid and energy transfer in different systems. The continuity, momentum, and energy equations can be obtained as follows:

$$\nabla \bullet \mathbf{u} = 0, \tag{2}$$

$$\frac{\partial \left(\rho_{nf}\mathbf{u}\right)}{\partial t} + \nabla \bullet \rho_{nf}\mathbf{uu} = -\nabla p + \mu_{nf}\nabla\left[\nabla\mathbf{u} + (\nabla\mathbf{u})^T\right] + \mathbf{g}\beta_{nf}\rho_{nf}\left(T - T_r\right), \tag{3}$$

$$\frac{\partial T}{\partial t} + \nabla \bullet \mathbf{u}T = \nabla \bullet \frac{k_{nf}}{\left(\rho C_p\right)_{nf}}\nabla T, \tag{4}$$

The dimensional analysis of the governing equations mentioned earlier reveals that the problem is primarily characterized by two dimensionless parameters: the Rayleigh number and the Prandtl number. The former is determined by the thermal buoyancy force (β), the gravitational acceleration (g), the height of the cavity (H), and the temperature difference between the hot and cold walls (T_h and T_c), divided by the product of kinematic viscosity (v), and thermal diffusivity (α), hence expressed as:

$$Ra = \frac{\beta g_y H^3 (T_h - T_c)}{v\alpha}, \tag{5}$$

Likewise, the latter is measured by the ratio of kinematic viscosity, v, to thermal diffusivity, α, as indicated:

$$Pr = \frac{v}{\alpha}, \tag{6}$$

For simulating nanofluids, a single-phase nanofluid model is employed. Specific details can be referred to in previous literature[24]. Table 1 displays the thermal properties of MWCNT-Fe_3O_4/water hybrid nanofluid at different volume fractions.

To quantitatively evaluate the heat transfer characteristics of the system and assess the impact of different parameters on these characteristics, we introduce the Nusselt number. The Nusselt number allows for the determination of the convective heat transfer rate by comparing the conductive and convective heat transfer at a fluid–solid interface. The local Nusselt number (Nu_{loc}) which is defined as

$$Nu_{loc} = -\left(\frac{k_{nf}}{k_f}\right)\left(\frac{\partial T}{\partial n}\right) \tag{7}$$

where n is the coordinate normal to the wall. In some cases, it is necessary to determine an average Nusselt number over a given time or spatial domain. The average Nusselt number, also called Nu_{ave}, is obtained by averaging Nu_{loc} over both time and space. Its value provides insight into the overall heat transfer characteristics of the system being studied. Importantly, it should be noted that for steady-state flow (when conditions within the system are unchanging over time), the average Nusselt number is solely determined by the spatial average of Nu_{loc}. This is because the time-averaged Nusselt number is equal to the steady-state Nusselt number.

4 Validation and Grid Independence

Figure 2 shows the isothermal lines and streamlines of a benchmark problem of natural convection inside a square cavity at different Rayleigh numbers. The present results can be compared with the works by Davis[25]. By comparison, it can be observed that both the isothermal lines and streamlines are consistent with the findings from previous literature. To quantitatively assess the accuracy of the obtained results, we performed calculations for natural convection inside a square cavity with a circular heat source. The average Nusselt number over the surface of the circular heat source was then calculated. Table 2 shows the comparisons of the average Nusselt numbers.

To select a suitable grid while ensuring computational accuracy and precision, a grid-independent study was conducted. The case of a circular heat source located above the cavity with $\varphi = 0.003$ and $Ra = 10^6$ was simulated using various grids. Table 3 illustrates the average Nusselt number

Table 1 Thermophysical properties of MWCNT-Fe_3O_4/water hybrid nanofluids [24]

ϕ	c_p (J kg^{-1} K^{-1})	μ(mPa·s)	k (W m^{-1} K^{-1})	ρ (kg/m^3)
0	4182	0.79	0.602	998.5
0.001	4182.66	0.91	0.6734	1002.34
0.003	4183.99	1.01	0.6856	1010.04

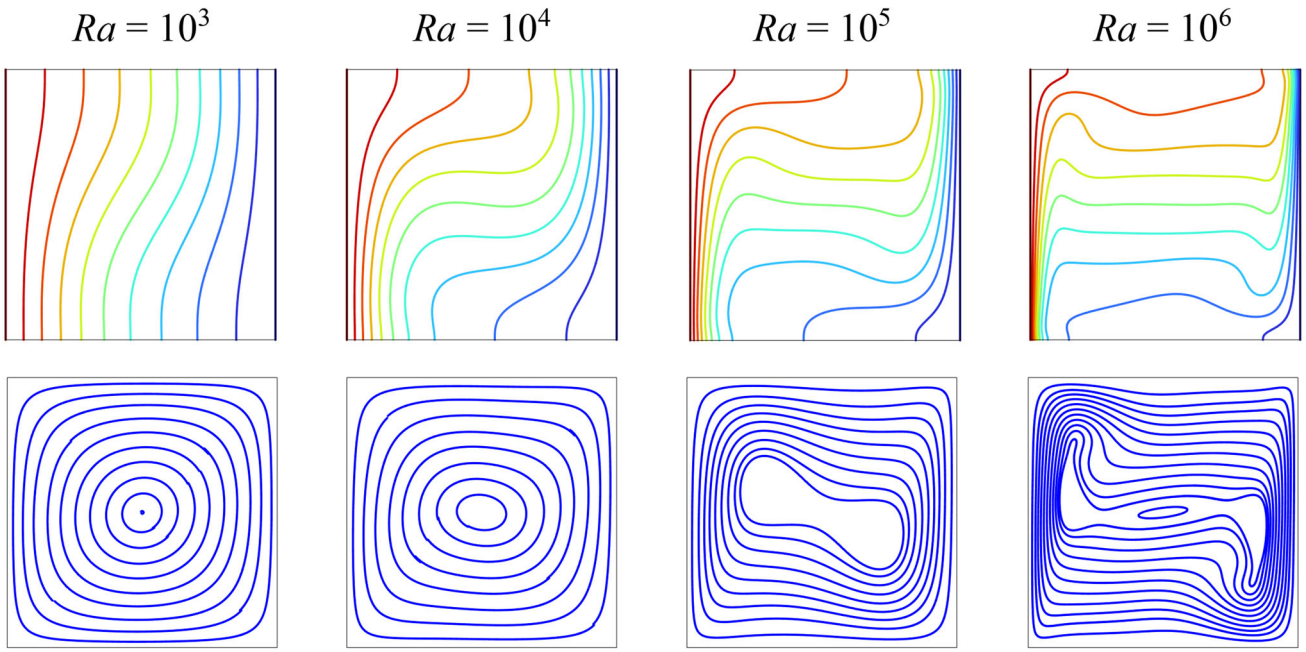

Fig. 2 The isothermal lines and streamlines by the present work [25]

Table 2 Comparisons of the average Nusselt numbers (Nu_{ave})

Ra	Present	Chen et al. [26]	Shu and Zhu [27]	Moukalled and Acharya [28]	Ren et al. [29]
10^3	3.156		–	–	–
10^4	3.214	3.263	3.24	3.331	3.161
10^5	4.889	4.968	4.86	5.08	4.836
10^6	8.868	9.195	8.90	9.374	8.546

Table 3 Average Nusselt number versus mesh number for $\varphi = 0.003$ and Ra $= 10^6$

Mesh number	Nu_{avg}	$100 \times \left\lvert \frac{Nu_{avg} - Nu_{old}}{Nu_{new}} \right\rvert$
738	11.675	
2145	13.787	15.318
16,785	14.950	7.779
21,461	14.952	0.013

obtained on the heated surface for different mesh numbers. From the figure, it can be observed that the difference in the average Nusselt numbers calculated for grid resolutions of 16,785 and 21,461 is 0.013. Therefore, to account for both the accuracy of the computational results and computational resources, the grid resolution of 16,785 is adopted.

5 Numerical Results and Discussions

In this section, we will investigate the effects of different Rayleigh numbers, volume fractions of nanofluids, positions of the heat source, and shapes of the heat source on flow dynamics, temperature fields, and heat transfer characteristics.

Figure 3 depicts the comparison of streamlines between the pure water ($\varphi = 0$) and nanofluid ($\varphi = 0.03$) for the case

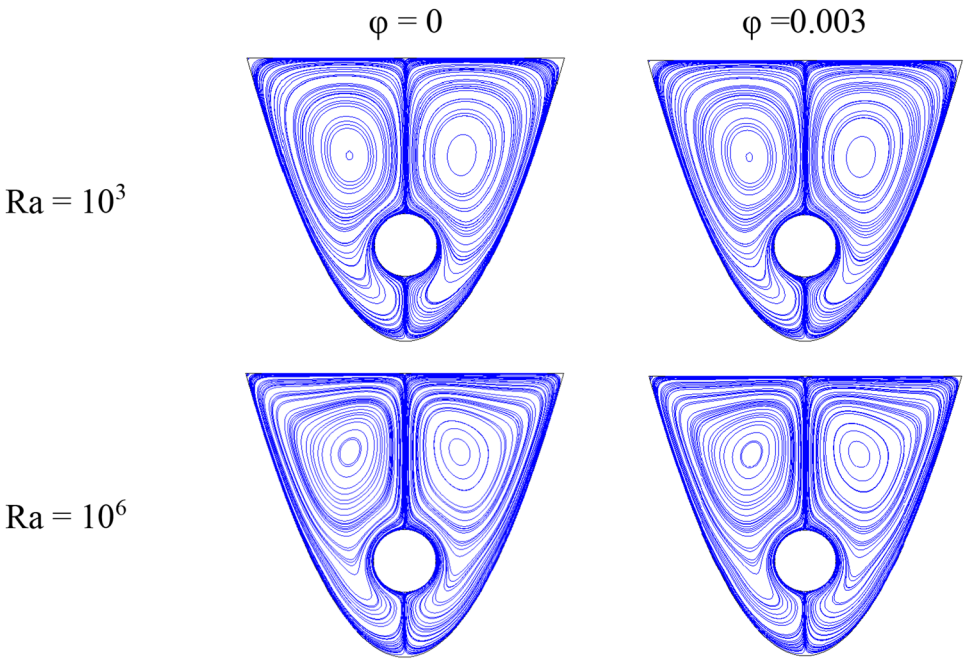

Fig. 3 Comparison of streamlines for the case when the circular heat source is located on the bottom of the cavity for different Ra

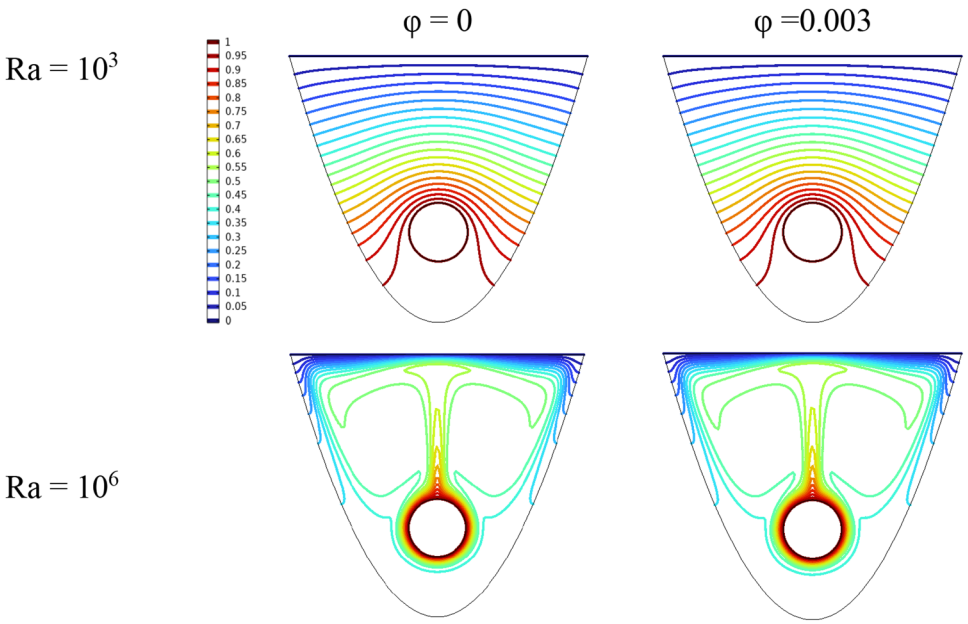

Fig. 4 Isothermal lines for the case when the circular heat source located on the bottom of the cavity for different Ra at $\varphi = 0$ and $\varphi = 0.003$

when the circular heat source located on the bottom of the cavity for low ($Ra = 10^3$) and high Rayleigh numbers ($Ra = 10^6$). Firstly, due to the symmetry of the geometry and the steady-state nature of the flow, the flow structure within the cavity is also symmetrical. At $Ra = 10^3$, the shape of the vortex is approximately elliptical, and the streamlines around the vortex are nearly identical, with only variations in size. When the Ra increases to 10^6, the shape of the streamlines in the inner and outer layers undergoes a change. The streamlines in the outer layer become closer to the shape of the wall boundary. This is due to the increase in convection intensity caused by the increase in the Rayleigh number. The subsequent analyses will involve a quantitative assessment of the impact of the nanofluid.

Figure 4 illustrates the isothermal lines for the case when the circular heat sources are located on the bottom for different Ra at $\varphi = 0$ and $\varphi = 0.003$. It should be noted that the color bar used in the temperature contour maps remains consistent. Therefore, the color bar will not be displayed in the subsequent sections. It can be observed that at $Ra = 10^3$, the main heat transfer mode is conducted through heat conduction due to the weak convective intensity and low flow

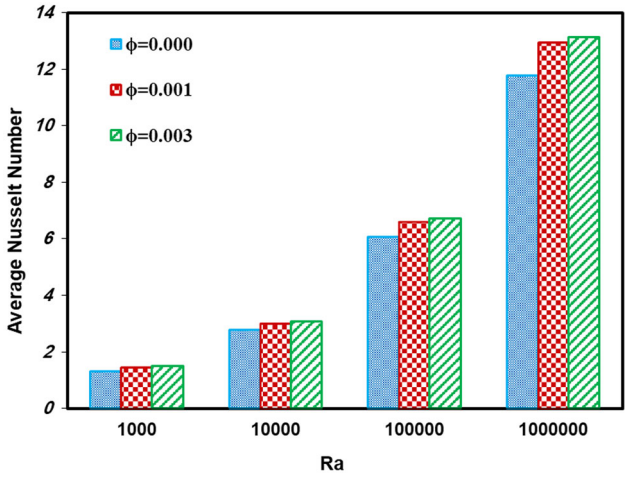

Fig. 5 The Nusselt number for the case when the circular heat source is located on the bottom for different φ and Ra

velocity within the cavity compared to Ra = 10^6. Therefore, the isotherms are relatively flat and evenly spaced. When the Ra increases to 10^6, thermal plumes form above the heat source and directly impinge on the top wall of the cavity, leading to the formation of two vortices on the left and right sides. It is worth noting that at high Rayleigh numbers, due to the generation of thermal plumes and the increase in convective intensity, the isotherms are no longer evenly distributed.

To quantitatively evaluate the heat transfer performance of the system, Fig. 5 presents the Nusselt number for the case when the circular heat source is located at the bottom for different values of φ and Ra. It can be observed that the average Nu increases with increasing φ and Ra. It is noteworthy that as Ra increases, the improvement in heat transfer characteristics achieved by using nanofluids becomes more pronounced compared to pure fluids.

On another hand, in addition to the Rayleigh number and the nanoparticle volume fraction φ, this paper also investigates the impact of the vertical position of the heat source. Figure 6 shows the streamlines and isothermal lines for the case when the circular heat source is located on the top of the cavity for different Ra at φ = 0. It can be observed that at Ra = 10^3 and 10^4, the streamlines and isothermal lines exhibit similar patterns. The distribution of the isothermal lines appears relatively uniform, without the presence of thermal plumes. However, as the Ra increases to 10^5 and 10^6, the isothermal lines become noticeably curved, indicating the presence of significant thermal plumes. The streamlines also indicate an evident increase in convection intensity. Based on the analysis above, it can be concluded that when the Ra is below 10^4, the dominant heat transfer mechanism is conduction.

On the other hand, when Ra exceeds 10^5, the primary heat transfer mechanism is thermal convection. Therefore, the critical Ra at which the transition between these two heat transfer mechanisms occurs lies between 10^4 and 10^5. Additionally, according to Fig. 3, it can be observed that when the heat source is located below the cavity, even at a high Ra number (10^6), only two vortices form within the cavity. However, when the heat source is positioned at the top (Fig. 6), in close proximity to the cold top wall, two smaller vortices form between the cold and heat sources. This corresponds to the presence of two thermal plumes at the top of the heat source.

Figure 7 shows the average Nusselt numbers at different φ and Ra values when the heat source is located at the top. By comparing Fig. 5 and Fig. 7, it can be observed that when the heat source moves from the bottom to the top, the average Nusselt number increases at any Ra value. This is because when the heat source is located at the top, it is closer to the cold source, leading to a significant improvement in heat transfer characteristics.

Figure 8 presents the streamlines and isothermal lines for the scenario where the circular heat source is positioned in the middle of the cavity, with Ra = 10^5 and φ = 0.001. From the streamlines and isothermal lines, it can be observed that thermal plumes have emerged, and the main mechanism of heat transfer is convection. This is consistent with the previous analysis, which indicates that the change in the heat transfer mechanism is mainly affected by the Rayleigh number, with little influence from the heat source position.

To further analyze the impact of the transition in heat transfer mechanisms on heat transfer efficiency, a plot of the variation in local Nusselt number along the surface of the heat source is depicted when the obstacle is in the middle of the cavity. Figure 9 illustrates the distribution of the local Nusselt number on the heated surface at φ = 0.001 for varying Rayleigh numbers. It can be clearly observed that the local Nusselt number remains relatively low and exhibits minimal variation when the Rayleigh number is equal to 10^3 and 10^4. However, for Ra = 10^5 and 10^6, the curve of Nu_{loc} exhibits a consistent pattern, featuring a trough corresponding to the location of thermal plumes on the heated surface. This is due to different heat transfer mechanisms. As above-mentioned, at Ra = 10^3, heat conduction is the primary heat transfer mechanism. As shown in Fig. 4, the isotherms are relatively evenly distributed, with the density of isotherms near the heat source directly above significantly higher than on both sides, resulting in a higher Nu_{loc}. However, when Ra = 10^6, the convective intensity significantly increases, forming plumes above the heat source, creating two vortices on the left and right. The cold fluid will impact the sides of the heat source, leading to higher Nu_{loc} on both sides. The occurrence of thermal plumes causes a significant increase in the Nu_{loc} in the surrounding area, resulting in a substantial enhancement of the average Nusselt number.

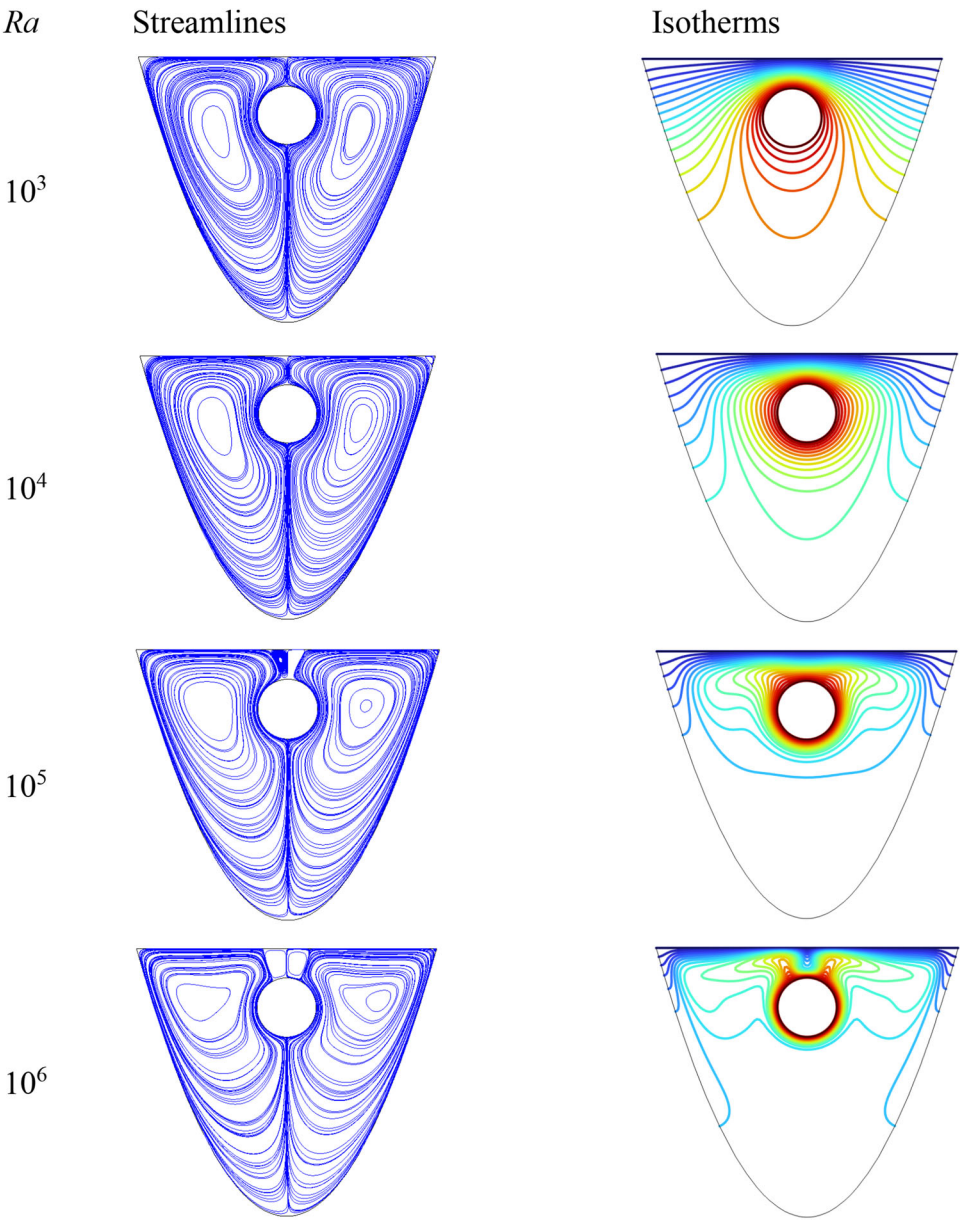

Fig. 6 Streamlines and isothermal lines for the case when the circular heat source is located on the top of the cavity for different Ra at $\varphi = 0$

Figure 10 shows the Nusselt number for the case when the circular heat source is located in the middle for different φ and Ra. By comparing with Fig. 5 and Fig. 7, it can be observed that when the heat source is positioned at the center of the cavity, the heat transfer characteristics also lie in the intermediate range. In other words, as the heat source moves upward from the bottom, there is an increase in the heat transfer characteristics.

The influence of the shape of the heat source was introduced in the following sections. Figure 11 shows the streamlines inside the cavity with circular and elliptic heat sources at $\varphi = 0.003$ and different Ra. As previously mentioned, when the heat source is circular, there is no need to elaborate further here; this section will focus solely on the impact of shape variations. When the shape of the heat source changes from circular to elliptical, the number of vortices remains unchanged, but the shape of the vortices differs due to variations in the boundary.

The similar changes can be observed in the temperature distribution. Figure 12 depicts the temperature distribution inside the cavity with circular and elliptical heat sources at $\varphi = 0.003$ and different Ra. When the heat source changes into an elliptical shape, at low Ra (10^3), the temperature distribution remains similar with only a change in shape. However, due to an increase in length in the horizontal direction, the distance at which thermal plumes occur increases at high Ra (10^6).

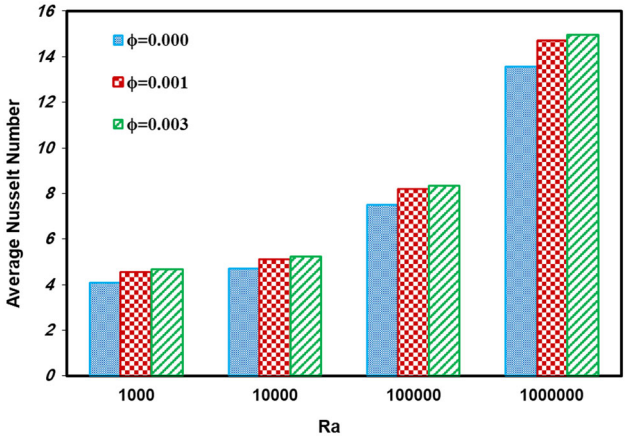

Fig. 7 The Nusselt number for the case when the circular heat source is located on the top for different φ and Ra

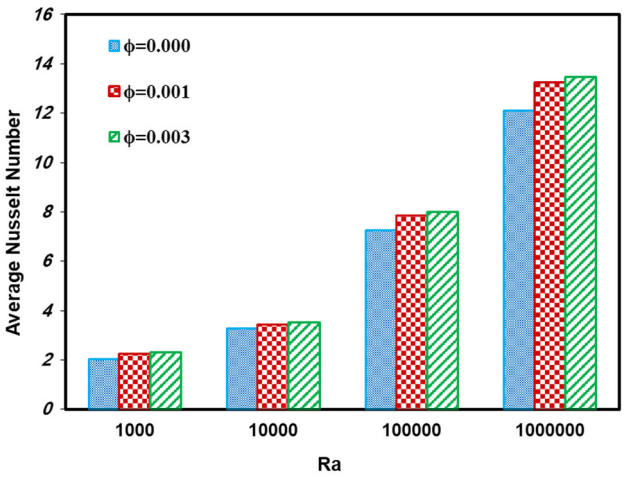

Fig. 10 The Nusselt number for the case when the circular heat source is located in the middle for different φ and Ra

Fig. 8 Streamlines and isothermal lines for the case when the circular heat source located in the middle of the cavity for Ra = $10.^5$ and φ = 0.001

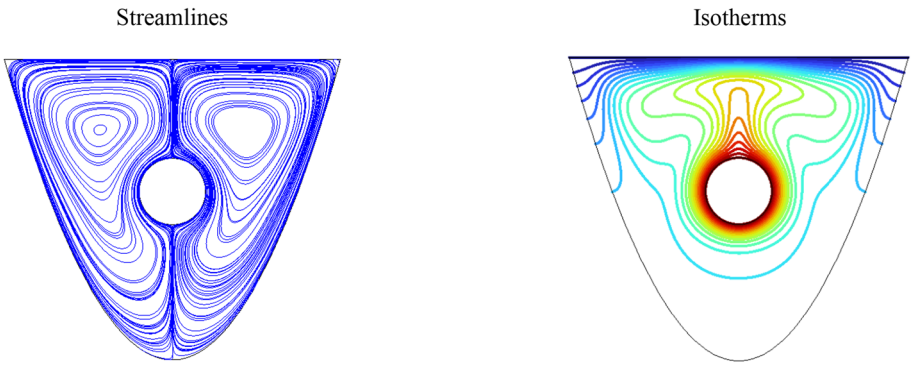

Fig. 9 The distribution of local Nusselt number on the heated surface at φ = 0.001 for different Ra

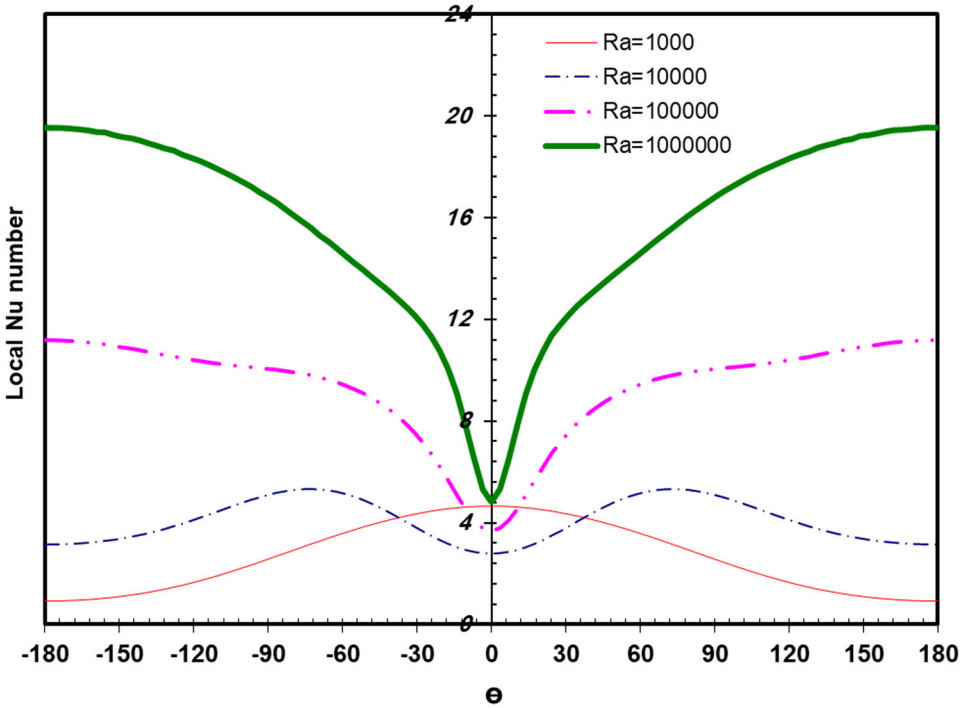

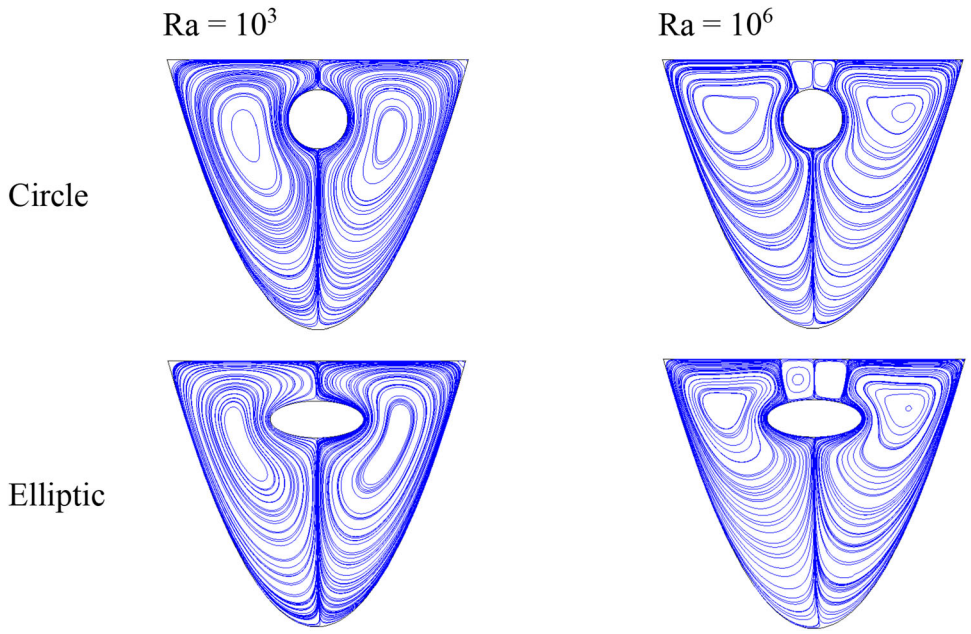

Fig. 11 Streamlines inside the cavity with a circular and elliptical heat source at $\varphi = 0.003$ and different Ra

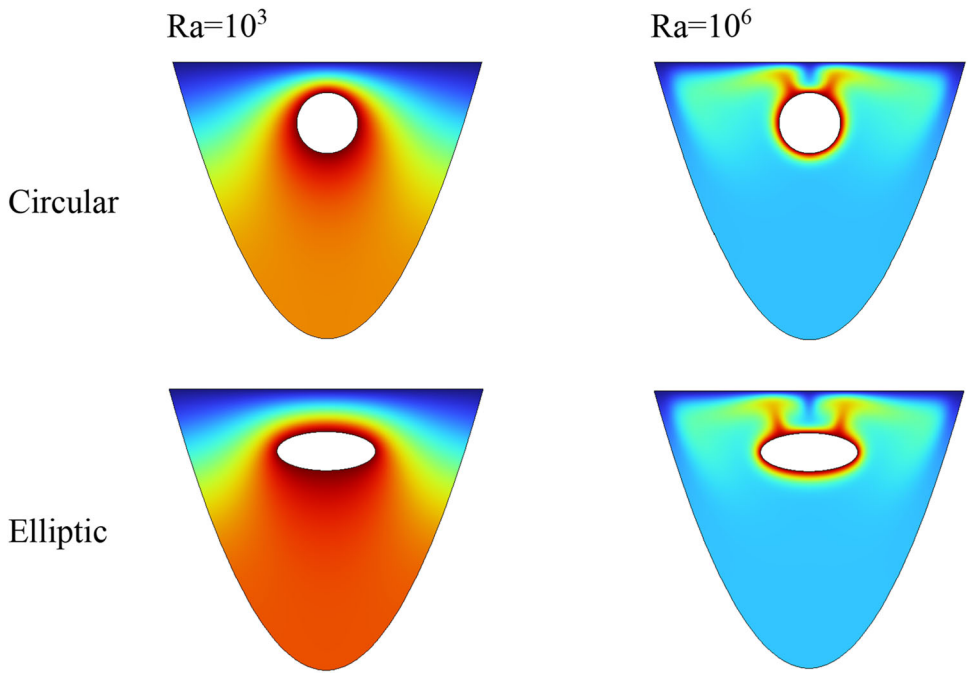

Fig. 12 Temperature distribution inside the cavity with circular and elliptical heat sources at $\varphi = 0.003$ and different Ra

Figure 13 shows the average Nusselt number of the circular and elliptical heat sources at $\varphi = 0.003$ and different Ra. It can be observed that Nu_{ave} increases with increasing Ra and φ, regardless of the circular or elliptical heat source. Moreover, at $Ra \leq 10^5$, the case with circular heat sources exhibits better heat transfer performance. However, at $Ra = 10^6$, the average Nusselt number of the elliptical heat source is higher than that of the circular one.

6 Conclusion

In this study, we investigate the natural convection of nanofluid inside a parabolic cavity with a heat source, which can be either circular or elliptical in shape. We analyze the impact of Ra, nanoparticle volume fraction, and heat source position on the convection process. Our observations reveal that the average Nusselt number increases with higher Rayleigh numbers and nanoparticle volume fractions. Additionally, relocating the heat source from the bottom region to the top area enhances its heat transfer performance. For

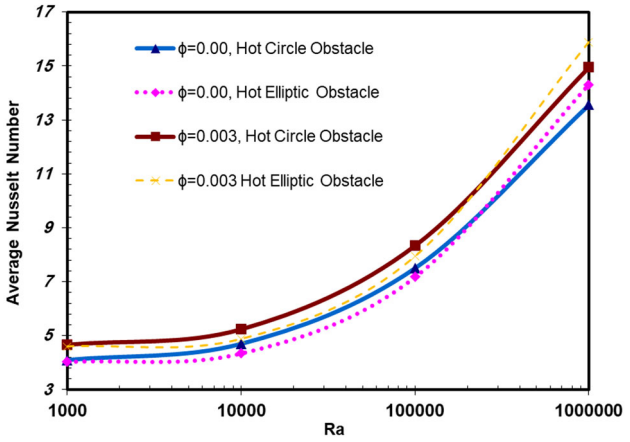

Fig. 13 The average Nusselt number of the circular and elliptical heat source at $\varphi = 0.003$ and different Ra

Rayleigh numbers less than or equal to 10^5, the circular heat source exhibits better heat transfer performance compared to the elliptical heat source. However, at a Rayleigh number of 10^6, the average Nusselt number of the elliptical heat source surpasses that of the circular one.

Funding Open access funding provided by The Hong Kong Polytechnic University.

References

1. Dong, Z.; Liu, P.; Xiao, H.; Liu, Z.; Liu, W.: A study on heat transfer enhancement for solar air heaters with ripple surface. Renew. Energy **1**(172), 477–487 (2021)
2. Mousa, M.H.; Miljkovic, N.; Nawaz, K.: Review of heat transfer enhancement techniques for single phase flows. Renew. Sustain. Energy Rev. **1**(137), 110566 (2021)
3. Yadav, R.J.; Mahajani, T.; Kore, S.S.; Gadhe, P.M.; Kamble, D.A.: Investigation of heat transfer characteristics using Fe_3O_4 nanofluid along with TT inserts in tube with uniform electromagnetic field. Appl. Nanosci. **13**(1), 763–785 (2023)
4. Ma, Y.; Mohebbi, R.; Rashidi, M.M.; Yang, Z.: Simulation of nanofluid natural convection in a U-shaped cavity equipped by a heating obstacle: effect of cavity's aspect ratio. J. Taiwan Inst. Chem. Eng. **1**(93), 263–276 (2018)
5. Ma, Y.; Mohebbi, R.; Rashidi, M.M.; Yang, Z.; Sheremet, M.A.: Numerical study of MHD nanofluid natural convection in a baffled U-shaped enclosure. Int. J. Heat Mass Transf. **1**(130), 123–134 (2019)
6. Hazarika, S.; Ahmed, S.; Yao, S.W.: Investigation of Cu–water nano-fluid of natural convection hydro-magnetic heat transport in a Darcian porous regime with diffusion-thermo. Appl. Nanosci. **13**(1), 283–293 (2023)
7. Ma, Y.; Mohebbi, R.; Yang, Z.; Sheremet, M.: Thermal performance of an environmentally friendly nanoliquid in a cabinet with two l-shaped heaters: application for electronic cooling. Int. J. Numer. Meth. Heat Fluid Flow **32**(12), 3637–3656 (2022)
8. Jebali, M.; Colangelo, G.; Gómez-Merino, A.I.: Green synthesis, characterization, and empirical thermal conductivity assessment of ZnO nanofluids for high-efficiency heat-transfer applications. Materials. **16**(4), 1542 (2023)
9. Giwa, S.O.; Sharifpur, M.; Meyer, J.P.: Experimental study of thermo-convection performance of hybrid nanofluids of Al2O3-MWCNT/water in a differentially heated square cavity. Int. J. Heat Mass Transf. **1**(148), 119072 (2020)
10. Goudarzi, S.; Shekaramiz, M.; Omidvar, A.; Golab, E.; Karimipour, A.; Karimipour, A.: Nanoparticles migration due to thermophoresis and brownian motion and its impact on Ag-MgO/Water hybrid nanofluid natural convection. Powder Technol. **20**(375), 493–503 (2020)
11. Reddy, N.K.; Swamy, H.K.; Sankar, M.; Jang, B.: MHD convective flow of Ag–TiO2 hybrid nanofluid in an inclined porous annulus with internal heat generation. Case Stud. Therm. Eng. **1**(42), 102719 (2023)
12. Yasir, M.; Khan, M.; Alqahtani, A.S.; Malik, M.Y.: Heat generation/absorption effects in thermally radiative mixed convective flow of Zn− TiO2/H2O hybrid nanofluid. Case Stud. Therm. Eng. **1**(45), 103000 (2023)
13. Chuhan, I.S.; Li, J.; Guo, Z.; Shahzad, H.; Yaqub, M.: Entropy optimization of MHD non-Newtonian fluid in a wavy enclosure with double diffusive natural convection. Numer. Heat Transfer., Part A: Appl. **21**, 1–21 (2023)
14. Rashid, U.; Shahzad, H.; Lu, D.; Wang, X.; Majeed, A.H.: Non-Newtonian MHD double diffusive natural convection flow and heat transfer in a crown enclosure. Case Stud. Therm. Eng. **1**(41), 102541 (2023)
15. Roy, N.C.; Monira, S.: Natural convection of a reacting hybrid nanofluid in an open porous cavity bounded by vertical wavy walls. Int. J. Numer. Methods Heat Fluid Flow **33**(9), 3202–3227 (2023)
16. Geridonmez, B.P.; Atilgan, M.A.: Numerical and machine learning approaches in nanofluid natural convection flow in a wavy cavity. Eng. Anal. Boundary Elem. **1**(155), 297–306 (2023)
17. Alazzam, A.; Qasem, N.A.; Aissa, A.; Abid, M.S.; Guedri, K.; Younis, O.: Natural convection characteristics of nano-encapsulated phase change materials in a rectangular wavy enclosure with heating element and under an external magnetic field. J. Energy Storage. **1**(57), 106213 (2023)
18. Saha, T.; Islam, T.; Yeasmin, S.; Parveen, N.: Thermal influence of heated fin on MHD natural convection flow of nanofluids inside a wavy square cavity. Int J Thermofluids. **1**(18), 100338 (2023)
19. Nabwey, H.A.; Rashad, A.M.; Reddy, P.B.; Jakeer, S.; Mansour, M.A.; Salah, T.: Radiative effects on unsteady MHD natural convection flow in an inclined wavy porous cavity using hybrid nanofluid containing a square obstacle. Alex. Eng. J. **15**(65), 921–937 (2023)
20. Kumar, S.; Mahapatra, S.K.: An experimental and numerical analysis of natural convection in a partially open cuboid enclosure with a cylindrical obstacle. Therm. Sci. Eng. Prog. **1**(45), 102118 (2023)
21. Franco, A.T.; Santos, P.R.; Lugarini, A.; Loyola, L.T.; De Lai, F.C.; Junqueira, S.L.; Nardi, V.G.; Ganzarolli, M.M.; Lage, J.L.: The effects of discrete conductive blocks on the natural convection

in side-heated open cavities. Appl. Therm. Eng. **25**(219), 119613 (2023)
22. Reddy, K.S.; Kumar, N.S.: Combined laminar natural convection and surface radiation heat transfer in a modified cavity receiver of solar parabolic dish. Int. J. Therm. Sci. **47**(12), 1647–1657 (2008)
23. Wu, S.Y.; Xiao, L.; Cao, Y.; Li, Y.R.: Convection heat loss from cavity receiver in parabolic dish solar thermal power system: a review. Sol. Energy **84**(8), 1342–1355 (2010)
24. Sundar, L.S.; Singh, M.K.; Sousa, A.C.: Enhanced heat transfer and friction factor of MWCNT–Fe_3O_4/water hybrid nanofluids. Int. Commun. Heat Mass Transfer **1**(52), 73–83 (2014)
25. de Vahl, D.G.: Natural convection of air in a square cavity: a bench mark numerical solution. Int. J. Numer. Meth. Fluids **3**(3), 249–264 (1983)
26. Chen, Z.; Shu, C.; Yang, L.M.; Zhao, X.; Liu, N.Y.: Immersed boundary–simplified thermal lattice Boltzmann method for incompressible thermal flows. Phys. Fluids (2020). https://doi.org/10.1063/15138711
27. Shu, C.; Zhu, Y.D.: Efficient computation of natural convection in a concentric annulus between an outer square cylinder and an inner circular cylinder. Int. J. Numer. Meth. Fluids **38**(5), 429–445 (2002)
28. Moukalled, F.; Acharya, S.: Natural convection in the annulus between concentric horizontal circular and square cylinders. J. Thermophys. Heat Transfer **10**(3), 524–531 (1996)
29. Ren, W.W.; Shu, C.; Wu, J.; Yang, W.M.: Boundary condition-enforced immersed boundary method for thermal flow problems with Dirichlet temperature condition and its applications. Comput. Fluids **30**(57), 40–51 (2012)